


Article

Study of SPRC Impact Resistance Based on the Weibull Distribution and the Response Surface Method

Song Chen , Ziling Xu, Zeli Liu, Chen Wang and JiuHong Jiang *

College of Civil Engineering, Architecture and Environment, Hubei University of Technology, Wuhan 430068, China; 102010881@hbut.edu.cn (S.C.); 101910580@hbut.edu.cn (Z.X.); 101910585@hbut.edu.cn (Z.L.); 102010862@hbut.edu.cn (C.W.)

* Correspondence: 19910019@hbut.edu.cn

Abstract: Silica-fume-polyvinyl-alcohol-fiber-reinforced concrete (SPRC) is a green and environmentally friendly composite material incorporating silica fume and polyvinyl alcohol fiber into concrete. To study the impact resistance of SPRC, compressive-strength and drop hammer impact tests were conducted on SPRC with different silica-fume and polyvinyl-alcohol-fiber contents. The mechanical and impact resistance properties of the SPRC were comprehensively analyzed in terms of the compressive strength, ductility ratio and impact-energy-dissipation variation. Based on the impact resistance of the SPRC, the impact life of SPRC with different failure probabilities was predicted by incorporating the Weibull distribution model, and an impact damage evolution equation for SPRC was established. The impact life of SPRC under the action of silica-fume content, polyvinyl-alcohol-fiber content and failure probability was analyzed in depth by the response surface method (RSM). The research results show that, when the content of silica fume is 10% and the content of polyvinyl alcohol fiber is 1%, the compressive strength and impact resistance of SPRC are the best. The RSM response model can effectively predict and describe the impact life of SPRC specimens under the action of three factors.

Keywords: silica fume; polyvinyl alcohol fiber; impact resistance; Weibull distribution model; response surface method



Citation: Chen, S.; Xu, Z.; Liu, Z.; Wang, C.; Jiang, J. Study of SPRC Impact Resistance Based on the Weibull Distribution and the Response Surface Method. *Polymers* **2022**, *14*, 2281. <https://doi.org/10.3390/polym14112281>

Academic Editors: Grzegorz Świt, Anna Adamczak-Bugno and Aleksandra Krampikowska

Received: 8 May 2022

Accepted: 30 May 2022

Published: 3 June 2022

Publisher's Note: MDPI stays neutral with regard to jurisdictional claims in published maps and institutional affiliations.



Copyright: © 2022 by the authors. Licensee MDPI, Basel, Switzerland. This article is an open access article distributed under the terms and conditions of the Creative Commons Attribution (CC BY) license (<https://creativecommons.org/licenses/by/4.0/>).

1. Introduction

Concrete is widely used in engineering as an integral part of the construction field [1,2]. For example, concrete is widely used in bridge structures, pile foundations, aircraft runways, dams and offshore platforms. However, these structures are subjected to various dynamic loads during their service, such as traveling loads [3–5], aircraft landings [6], waves [7], earthquakes [8], and other dynamic loading effects. These unavoidable human [9–11] and natural factors [12] present serious challenges to the safety of concrete structures. Therefore, it is important to study the impact resistance of concrete structures under various impact loads for disaster prevention and mitigation.

Currently, the problem of how to enhance the impact resistance of concrete has been widely studied by researchers. To enhance impact resistance, some researchers have incorporated fibers in concrete [13]. Examples include steel fibers [14,15], carbon fibers [16], recycled glass fibers [17], polypropylene fibers [18], and natural plant fibers [19]. Some researchers have found that adding different aggregates can enhance the impact resistance of concrete. For example, Wu et al. [16] found that larger and higher strength coarse aggregates can improve the impact resistance of concrete. Zhang et al. [20] found that bauxite coarse aggregates are beneficial for improving the mechanical properties and impact resistance of cement composites. Mustafa et al. [21] concluded that the impact strength of concrete increases with the percentage of plastic waste replacing sand. Vatin [22] found that the use of asphalt-mixed aggregates can improve the impact power of concrete.

Silica fume is the industrial waste produced by ferroalloying plants. Incorporation of silica fume in concrete can reduce the amount of cement and save mineral resources. The reuse of silica fume can improve the environment, save energy, reduce emissions and reduce secondary pollution. Importantly, silica fume has high activity, pozzolanic activity and a microaggregate filling reaction, which can improve the mechanical properties and durability of concrete [23]. Silica fume is commonly used in UHPC to improve mechanical properties, and the cement replacement ratio of silica fume is typically within 20% [24]. Although Luan et al. [25] found that the drying shrinkage of UHPC increased with the increase of silica fume content, some scholars have found that the incorporation of a small amount of silica fume has many advantages [26–31]. Poon et al. [26] found that, with the incorporation of silica fume, the compressive strength and chloride ion penetration resistance of concrete were improved. Hassani et al. [27] found that, with the incorporation of silica fume, the mechanical properties of pavement-panel concrete improved significantly. Alaloul et al. [28] found that the incorporation of silica fume compensates for the loss of mechanical properties due to the incorporation of rubber. Liu et al. [29] compared the test results of concrete with silica fume incorporated, with concrete without silica fume, and found that the strength of the concrete increased with the incorporation of the silica fume. Zhao et al. [30] incorporated silica fume into concrete and showed through a series of experiments that the impact resistance of concrete was improved with the incorporation of silica fume. Shafaghat et al. [31] used electron microscopy to analyze the internal structure of silica-fume concrete. The analysis showed that silica fume improved the microstructure of concrete during the hydration of cement with a simultaneous pozzolanic reaction.

Polyvinyl alcohol (PVA) fiber is a synthetic fiber with acid resistance, alkali resistance, high strength and high modulus. As a reinforcing fiber, it has the advantages of high deformation capacity, superior tensile properties and excellent fracture properties, which have been recognized by the material-science and engineering community [32–34]. Li et al. [35] found that the concrete fracture-damage process becomes longer with the incorporation of polyvinyl alcohol fibers. Zhang et al. [36] found that the incorporation of polyvinyl alcohol fibers enhanced the splitting tensile strength and flexural strength of concrete. Qiu et al. [37] found that polyvinyl alcohol fibers effectively retarded the fatigue damage of concrete. Kim et al. [38] placed polyvinyl alcohol fiber concrete in a harsh environment for a period of time and scanned its permeable pores and carbonation depth using electron microscopy, and the results showed that polyvinyl alcohol fiber concrete exhibited a better durability performance. Afroughsabet et al. [39] found that, with the incorporation of polyvinyl alcohol fibers, the dry shrinkage of concrete during precuring significantly decreased. Chen et al. [40] found that the incorporation of polyvinyl alcohol fibers significantly enhanced the blast resistance of concrete. Zhao et al. [41] placed polyvinyl-alcohol-fiber concrete in a freeze–thaw environment and subjected samples to a sulfate attack in a seawater environment. They found that the concrete durability was significantly enhanced with the incorporation of polyvinyl alcohol fibers.

Some scholars have improved the mechanical properties and durability of concrete by mixing fiber and mineral materials [42–45]. Mosavinejad et al. [42] prepared ultrahigh-performance concrete with a high content of silica fume and short-cut polyvinyl alcohol fibers and concluded that, for compressive strength, the optimum ratio of silica fume to cement is 0.3, a further increase in silica fume content leads to a decrease in compressive strength, and the incorporation of PVA fibers reduces the diffusion and penetration of chloride ions. Prakash et al. [43] studied the mechanical properties and resistance to chloride ion penetration of UHPC containing silica fume and finely ground slag. Satnam et al. [44] found that mixing scrap tire rubber and silica fume can improve the impact resistance of concrete. Suruchi Mishra et al. [45] studied the impact resistance of ultrahigh-performance fiber-reinforced concrete mixed with silica fume and fiber components, and they found that the UHPFRC impact response depends heavily on the energy and velocity of the impact mass, specimen size, support stiffness, test type, and even the definition of damage. However, there are few in-depth analyses of the impact-damage process and

impact life of concrete mixed with mineral materials and fibers. The purpose of this study is to predict the impact life of SPRC with different failure probabilities with the Weibull distribution model. The SPRC impact-damage evolution equation was established to study the damage evolution trend of SPRC impact life under repeated impact. The effects of silica-fume content, polyvinyl-alcohol-fiber content and failure probability on SPRC impact life were analyzed with the response surface method (RSM).

2. Materials and Methods

2.1. Materials

The cement was P.O 42.5 grade ordinary silicate cement from Wuhan Xinhua Company. The aggregates were from Wuhan. The coarse aggregate was ordinary graded gravel with particle size of 5 to 25 mm. The fine aggregate was Grade II medium sand with continuous grading and a fineness modulus of 2.83. The fly ash was Grade I fly ash from Henan Hengyuan New Materials Co. Ltd. The silica fume was produced by Henan Yixiang New Materials Co. Ltd. Polyvinyl alcohol fiber was produced by Kuraray Japan. The detailed parameters of silica fume, fly ash, cement and polyvinyl alcohol fiber are shown in Table 1. Polyvinyl alcohol fiber and silica fume are shown in Figure 1. The water-reducing agent was a polycarboxylic-acid high-performance water-reducing agent. The test water was ordinary tap water.

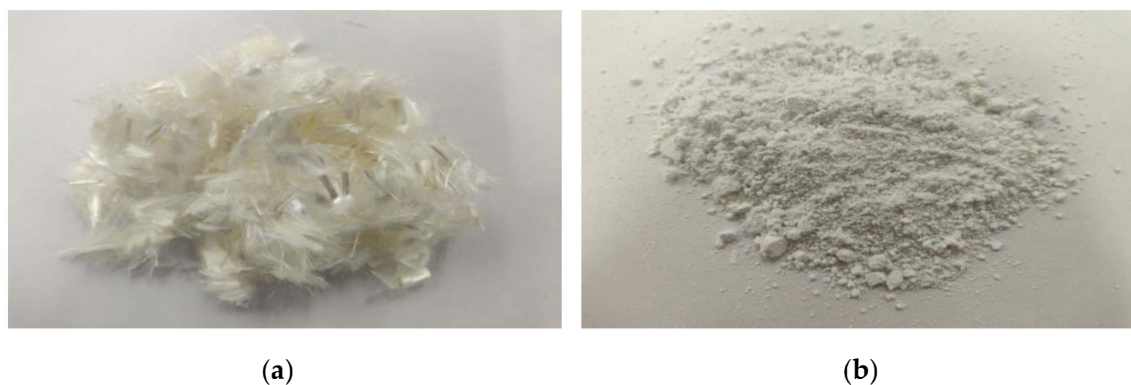


Figure 1. (a) Polyvinyl alcohol fiber; (b) silica fume.

Table 1. Detailed parameters of silica fume and polyvinyl alcohol fiber.

Silica fume	SiO ₂ (%)	Loss of ignition (%)	Specific surface area (m ² /g)	Chloride ion (%)	28 d activity index (%)
	98.1	1.48	21	0.01	105
Fly ash	Fineness (%)	Burning vector (%)	Water content (%)	Density (g/cm ³)	Bulk density (g/cm ³)
	16	2.8	0.85	2.55	1.12
Cement	Standard consistency water consumption (%)	Initial setting time (min)	Final setting time (min)	Cube compressive strength (MPa)	
				7 d	28 d
	26.6	196	265	25.8	44.5
Polyvinyl alcohol fiber	Fiber diameter (μm)	Fiber length (mm)	Tensile strength (MPa)	Elongation at break (%)	Cross-sectional expansion rate (cN/dtex)
	31	9	1400–1600	17 ± 3.0	320

2.2. Concrete Mixing Ratio Design

The SPRC was based on C40 concrete (the cube compressive strength of 150mm side length was 40 MPa) as the base mix ratio. The 100 mm × 100 mm × 100 mm cubed

specimens were taken for the compressive-strength test, and three specimens were made from each group. Cylindrical Φ 150 mm \times 63 mm specimen test blocks were taken for the drop-hammer impact tests, and six specimens were made from each group. The water-binder ratio was 0.43, the content of the silica fume (0%, 5%, 10%, 15%) was varied by cement weight, and the content of polyvinyl alcohol fibers (0%, 0.5%, 1%, 1.5%) was varied by the volume of the entire mixture. The water-reducing agent content was 1 kg/m³. The mixing proportion is shown in Table 2.

Table 2. Mix proportions of the designed concrete.

NO.	Polyvinyl Alcohol Fiber/%	Content of Material (kg/m ³)						Water-Reducing Agent
		Silica Fume	Cement	Coarse Aggregate	Sand	Fly Ash	Water	
SPRC-0-0 *	-	-	330	1061	837	61	170	1
SPRC-0.5-5	0.5	16.5	313.5	1061	837	61	170	1
SPRC-0.5-10		33	297	1061	837	61	170	1
SPRC-0.5-15		49.5	280.5	1061	837	61	170	1
SPRC-1-5	1	16.5	313.5	1061	837	61	170	1
SPRC-1-10		33	297	1061	837	61	170	1
SPRC-1-15		49.5	280.5	1061	837	61	170	1
SPRC-1.5-5	1.5	16.5	313.5	1061	837	61	170	1
SPRC-1.5-10		33	297	1061	837	61	170	1
SPRC-1.5-15		49.5	280.5	1061	837	61	170	1

* SPRC-0-0 means that the content of silica fume is 0 and the volume content of polyvinyl alcohol fiber is 0. The latter groups, and so on.

2.3. Specimen Production and Test Methods

The specimens were prepared by an HJS-60 type twin-shaft concrete test mixer. Considering that polyvinyl alcohol fibers tend to agglomerate, the fibers were torn and dispersed by hand before being added to the mixer. In the mixing process, the first step was to add gravel and sand and mix for 1 min; then, cement, fly ash and silica fume were added and mixed for 1 min; finally, part of the water and the water-reducing agent were added and mixed for 2 min. The second step was to add the treated polyvinyl alcohol fiber evenly into the mixer and to continue to mix for 2 min after adding; then, the remaining water and water-reducing agent were added and mixing was continued for 2 min. To avoid uneven distribution of polyvinyl alcohol fiber in the concrete, the mixing time was extended appropriately. After mixing, the mix was poured into molds for full pounding. After pounding, the specimens were placed in a cool place for 24 h to demold, and the specimens were stored in a standard maintenance room for maintenance treatment.

The compressive-strength tests were performed according to the standards specified in GB/T 50081-2019 [46] and CECS 13:2009 [47]. The compressive-strength test of the cube specimens with a size of 100 mm \times 100 mm \times 100 mm was carried out by using the DYE-2000S microcomputer servo pressure testing machine. The specific operation method of the compression test was as follows: after the end of specimen maintenance, the specimen was promptly removed, excess water on the surface of the specimen was wiped off, and the appearance of the specimen was verified to meet the requirements. As the concrete strength was C40, according to the specification, the loading speed of this test was 0.5 MPa/s. After the specimen was destroyed, the test was stopped and the test results were recorded.

The impact test method adopted was the drop-hammer impact test method recommended by the American Concrete Association ACI 544 standard [48]. The method has the advantages of simple operation and relatively low test-condition requirements. This test adopts a CECS13-2009 drop-hammer impact testing machine to test the impact resistance of the specimen, as shown in Figure 2. The test method was as follows: a Φ 150 mm \times 63 mm cylindrical specimen

was placed in four baffles on the chassis, the specimen was 5 mm from the baffle, and a Φ 63 mm steel ball was placed on the specimen. The height of the hammer drop of the test device was fixed at the standard height, and the distance between the center of mass of the hammer and the surface of the steel ball on the test block was 500 mm. The electromagnetic switch that controls the drop hammer has a counter connected to it. The button on the electromagnetic switch controls the drop hammer for impact, and the counter records the number of impacts with each press of the button. As the number of impacts increased, when the first visible crack appeared in the specimen was regarded as the first crack, and the number of impacts at this time was recorded. When the specimen was impacted and fully cracked such that the specimen touched the three surrounding baffles, this was regarded as the final crack, and the number of impacts was recorded at this time.

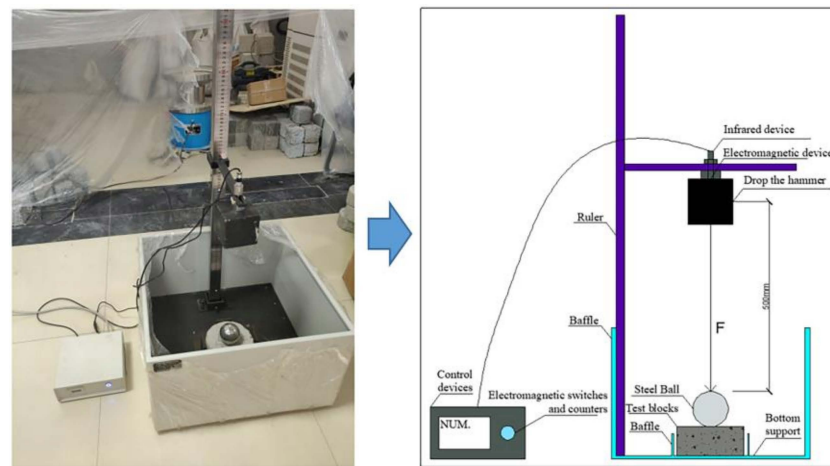


Figure 2. Drop-hammer impact device.

3. Results

3.1. Compressive Strength of SPRC

The compressive-strength test results and compressive-strength changes are shown in Figure 3. The error bars in the figure are the standard deviations, and the error bars indicate the dispersion of the data; smaller error bars indicate smaller data dispersion. When the silica fume content was 10%, the overall growth rate of the compressive strength of SPRC was the highest. This is because of the small silica-fume size and its microaggregate filling effect, which can play a role in filling the small pores inside the cementitious composites. The incorporation of silica fume reduces the porosity and improves the internal structure. The interfacial transition zone of cement-matrix composites is often the weak region of their internal structure due to the large number of $\text{Ca}(\text{OH})_2$ crystals attached to the interfacial transition zone, which leads to the increased porosity and looser network structure in this region. Silica fume has high volcanic ash activity. The SiO_2 in silica fume can react with $\text{Ca}(\text{OH})_2$ crystals produced by cement hydration to generate a C-H-S gel by a secondary hydration reaction, which reduces the pore volume and pore distribution in the interfacial transition zone and improves the network structure in this region, increasing the compressive strength.

With the increase in polyvinyl alcohol fiber content, the compressive-strength growth rate of SPRC was also significantly improved. This is because, when the specimen is subjected to load, the stress is often formed at the crack tip inside the specimen. With continuous loading, the stress at this tip also increases, leading to the extension of cracks inside the specimen, thus forming more cracks and eventually causing damage to the specimen. The polyvinyl alcohol fiber bridging effect exists, and fiber incorporation will form a complex force system in the concrete. This causes the concrete to be subjected to an external load, and polyvinyl alcohol fiber will form a reverse stress at the crack tip to offset part of the energy generated by the

external load, thereby delaying the growth and extension of cracks so that the tolerance has been increased, and the strength has been improved.

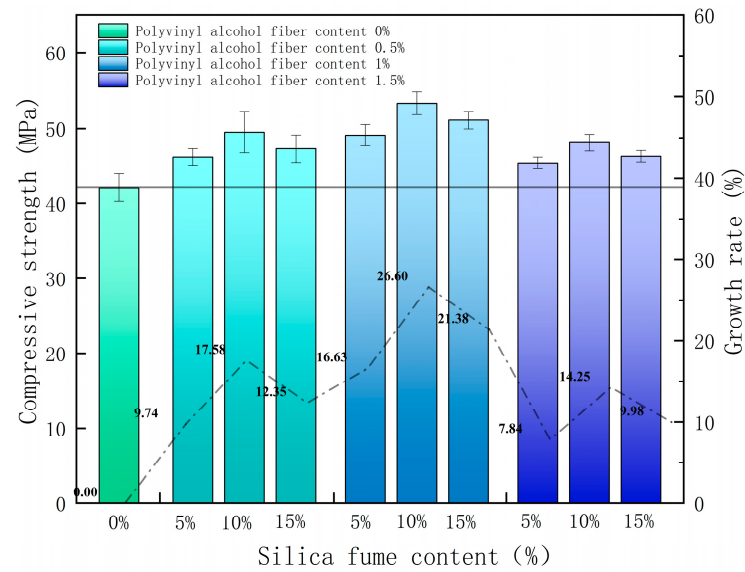


Figure 3. Compressive-strength growth of the SPRC.

However, a high silica-fume content and a high polyvinyl-alcohol-fiber content are not always better. When the content of silica fume exceeds 10%, the compressive-strength growth rate of the SPRC begins to decline. This is because the specific surface area of the silica-fume particles is large. When the silica-fume content is too large, silica-fume particles will adsorb more free water in cement composites. This reduces the content of water involved in the cement hydration reaction, and the hydration degree of the cement-based composites decreases, resulting in a downward trend in the compressive strength with a continuous increase in silica-fume content. When the polyvinyl-alcohol-fiber content is more than 1%, the compressive-strength growth rate of the SPRC also shows a downward trend, which is due to excessive fiber content that makes the cementitious material unable to be fully wrapped, which causes stress defects inside the specimen, resulting in compressive strength decreases with increasing polyvinyl alcohol fiber content.

3.2. SPRC Impact Resistance

The strength of the impact resistance of SPRC is reflected by the impact energy consumption W and ductility ratio λ . The equation for impact energy consumption W is shown in Equation (1), and the equation for the ductility ratio λ is shown in Equation (2). The test results for the number of impacts that caused the first visible cracks N_1 and the number of impacts that caused the ultimately failure of the specimens N_2 are shown in Table 3. The SPRC impact damage pattern is shown in Figure 4.

$$W = N_2 mgh \tag{1}$$

In Equation (1): W —impact energy consumption (J);

N_2 —the number of impacts that caused the ultimate failure of specimens (times);

m —impact hammer quality (kg), 4.5 kg;

g —gravitational acceleration (m/s^2), $9.81 m/s^2$;

h —drop height (m), 0.5 m.

$$\lambda = \frac{N_2 - N_1}{N_1} \tag{2}$$

In Equation (2): λ —Ductility ratio, N_1 —the number of impacts to cause the first visible cracks, and N_2 —the number of impacts that caused the ultimate failure of the specimens.

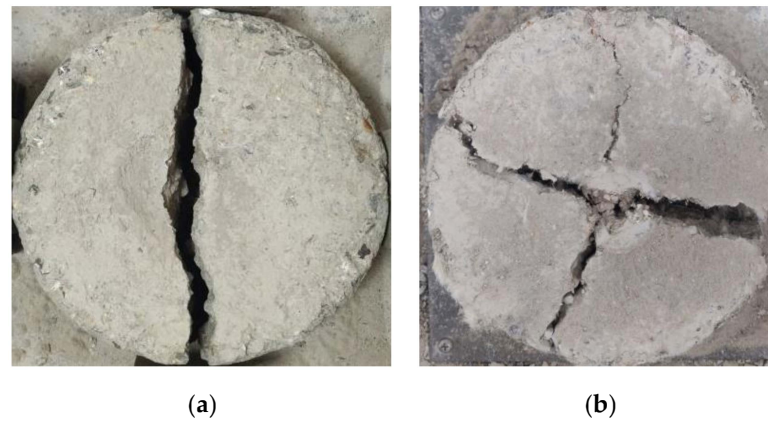


Figure 4. (a) Impact rupture form in ordinary concrete; (b) impact rupture form in SPRC.

Table 3. N_1 and N_2 under concrete drop-hammer impact.

NO.	N_1/N_2					
	1	2	3	4	5	6
SPRC-0-0	574/575	733/734	674/676	788/789	812/814	805/806
SPRC-0.5-5	1278/1288	1156/1168	1380/1388	1403/1410	1448/1462	1153/1166
SPRC-0.5-10	1356/1372	1212/1226	1577/1591	1425/1436	1384/1393	1478/1491
SPRC-0.5-15	1231/1242	1422/1435	1187/1201	1376/1384	1403/1412	1457/1472
SPRC-1-5	1643/1657	1571/1582	1432/1449	1527/1542	1554/1567	1495/1510
SPRC-1-10	1908/1928	1856/1873	1744/1762	1872/1887	1793/1810	1891/1907
SPRC-1-15	1778/1803	1603/1616	1677/1687	1568/1580	1732/1748	1530/1542
SPRC-1.5-5	1248/1258	1321/1330	1156/1168	1227/1238	1176/1189	1078/1085
SPRC-1.5-10	1474/1488	1531/1543	1243/1256	1278/1289	1341/1353	1185/1193
SPRC-1.5-15	1315/1327	1144/1154	1287/1296	1173/1185	1248/1257	1195/1207

As seen from Table 3, due to the large discreteness of concrete itself, the discreteness of the results of the number of impacts to cause the first visible cracks N_1 and the number of impacts that caused the ultimate failure of the specimens N_2 is also large, and the results of six specimens in each group were averaged. According to Equations (1) and (2), the impact energy consumption W and ductility ratio λ were calculated. The results are shown in Table 4, and the change in impact energy consumption W is shown in Figure 5. The error bars in the figure are the standard deviations, and the error bars indicate data dispersion: smaller error bars indicate smaller data dispersion.

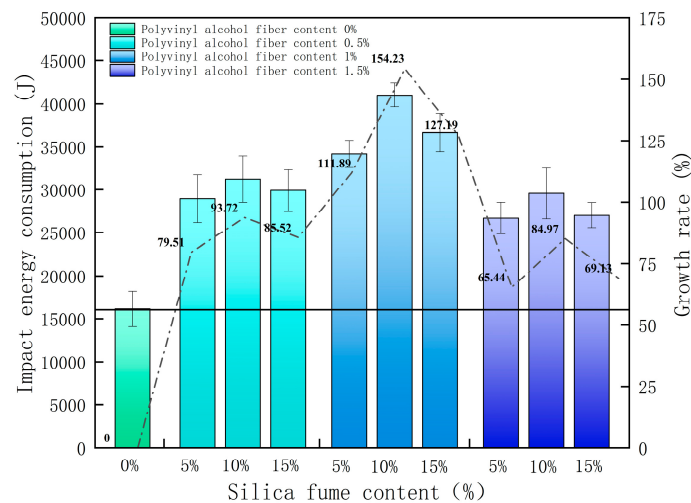


Figure 5. Growth in SPRC impact energy consumption.

Table 4. Impact resistance index analysis results.

NO.	Average Number of Impact Resistance			λ (%)	W (J)	Growth Rate of W (%)
	N_1	N_2	$N_2 - N_1$			
SPRC-0-0	731	732	1	0.14	16,157.07	0.00
SPRC-0.5-5	1303	1314	11	0.84	29,003.27	79.51
SPRC-0.5-10	1405	1418	13	0.93	31,298.81	93.72
SPRC-0.5-15	1346	1358	12	0.89	29,974.46	85.52
SPRC-1-5	1537	1551	14	0.91	34,234.45	111.89
SPRC-1-10	1844	1861	17	0.92	41,076.92	154.23
SPRC-1-15	1648	1663	15	0.91	36,706.57	127.19
SPRC-1.5-5	1201	1211	10	0.83	26,729.80	65.44
SPRC-1.5-10	1342	1354	12	0.89	29,886.17	84.97
SPRC-1.5-15	1227	1238	11	0.90	27,325.76	69.13

Table 4 shows that the ductility ratio of SPRC is significantly improved. Compared with the benchmark concrete, SPRC often experiences multiple drop-hammer impacts before the ultimate failure, which indicates that the combination of silica fume and polyvinyl alcohol fiber can enhance the ductility of SPRC. Figure 5 shows that, with the increase in silica-fume content, the impact energy consumption of SPRC first increases and then decreases, and when the silica fume content is at 10%, the impact energy consumption reaches the maximum.

After the specimen is subjected to repeated drop-hammer impacts, the internal cracks will extend and expand after the impact load. With the increasing number of impacts, the damage deterioration inside the concrete will gradually intensify, and the specimen will eventually experience failure damage. Figure 5 shows that, with the increase in polyvinyl alcohol fiber content, the impact energy consumption of SPRC first increases and then decreases, and when the polyvinyl-alcohol-fiber content is at 1%, the impact energy consumption reaches the maximum. When the silica-fume content was 10% and the polyvinyl alcohol fiber content was 1%, the impact resistance of SPRC was the best and was 154.32% higher than that of the benchmark concrete.

3.3. Impact Resistance Analysis of SPRC Based on the Weibull Distribution Model

3.3.1. SPRC Impact Life Analysis

Due to a large number of irregular microcracks, micropores and other defects in concrete, the damage to a concrete structure under repeated drop-hammer impacts has great randomness. Impact damage can be regarded as a kind of random distribution variable that must conform to a certain statistical law. The Weibull distribution model [49–51] has been widely used for life prediction in the failure assessment of brittle materials. Therefore, with the number of final cracks of the SPRC as the original data, the Weibull distribution model was selected to explore the impact life changes of the SPRC under different failure probabilities. The Weibull distribution model is a three-parameter function proposed by Waloddi Weibull in the study of material fatigue life, as shown in Equation (3):

$$f(x) = \frac{\beta}{\eta} \left(\frac{x - x_0}{\eta} \right)^{\beta-1} \exp \left[- \left(\frac{x - x_0}{\eta} \right)^{\beta} \right] \quad (x \geq x_0) \quad (3)$$

In Equation (3): β —Shape factor;

η —Scale factor;

x_0 —Location parameters ($x_0 \geq 0$).

Due to the similarity of the failure mechanism between the impact failure and fatigue failure of specimens, the impact life N also obeys the Weibull distribution, but the three parameters of the original function need to be redefined. Let the original parameters $\beta = b$, $\eta = N_a - N_0$ and $x_0 = N_0$; then, the specimen impact life N can be expressed by the following probability density function, Equation (4):

$$f(N) = \frac{b}{N_a - N_0} \left(\frac{N - N_0}{N_a - N_0} \right)^{b-1} \exp \left[- \left(\frac{N - N_0}{N_a - N_0} \right)^b \right] \quad (\infty > N \geq N_0) \quad (4)$$

In Equation (4): b —Weibull shape parameters;

N_0 —Minimum life parameter;

N_a —Characteristic life parameters.

Its cumulative distribution function $F(N_p)$ is expressed by Equation (5):

$$F(N_p) = P_1(N < N_p) = \int_{N_0}^{N_p} f(N)dN = 1 - \exp \left[- \left(\frac{N_p - N_0}{N_a - N_0} \right)^b \right] \quad (5)$$

In Equation (5), $P_1(N < N_p)$ indicates the probability of being less than a certain value N_p . The value of the function corresponding to the cumulative distribution function $F(N_p)$ is called the cumulative probability of failure, from which the reliability function P_2 can be expressed as:

$$P_2 = P_1(N > N_p) = 1 - F(N_p) = \exp \left[- \left(\frac{N_p - N_0}{N_a - N_0} \right)^b \right] \quad (6)$$

After determining the survival rate P_2 , the impact life N_p under the corresponding failure probability P_1 can be calculated from Equation (6). Considering the safety and reliability of the specimen in the service process and the simplified calculation, the minimum life parameter N_0 is set to 0, and the two-parameter Weibull probability density function is obtained. The function expression is expressed as Equation (7):

$$f(N) = \frac{b}{N_a} \left(\frac{N}{N_a} \right)^{b-1} \exp \left[- \left(\frac{N}{N_a} \right)^b \right] \quad (\infty > N \geq N_0) \quad (7)$$

Then, the failure probability function P_1 for $N > N_p$ is shown in Equation (8):

$$P_1 = 1 - \exp \left[- \left(\frac{N}{N_a} \right)^b \right] \quad (8)$$

The survival rate function P_2 is calculated by Equation (9):

$$P_2 = 1 - P_1 = \exp \left[- \left(\frac{N}{N_a} \right)^b \right] \quad (9)$$

Taking the natural logarithm twice for both sides of Equation (9), Equation (10) is obtained.

$$\ln \left[\ln \left(\frac{1}{P_2} \right) \right] = b \ln \left(\frac{1}{N_a} \right) + b \ln(N) \quad (10)$$

Let $y = \ln \left[\ln \left(\frac{1}{P_2} \right) \right]$, $x = \ln(N)$, $a = b \ln N_a$ and $N_a = \exp[-(a/b)]$; then, we can obtain Equation (11):

$$Y = a + bX \quad (11)$$

Equation (10) can be used to test whether the test data obey the distribution law of the Weibull probability density function, and the test data are subjected to linear regression analysis to find the parameters a and b . After linear regression analysis of the test data, whether there is a good linear relationship between Y and X is tested by combining the two parameters. If there is, the Weibull probability density function can reasonably predict and describe the impact life of SPRC under different failure probabilities. If not, the Weibull probability density function is not applicable to the impact life analysis of SPRC.

To verify whether the impact life of specimens conforms to the Weibull distribution, there should be a good performance relationship between $\ln[\ln(1/P_2)]$ and $\ln(N)$. The survival rate P_2 needs to be calculated first, and the calculation method is shown in Equation (12):

$$P_2 = 1 - \frac{i}{m + 1} \tag{12}$$

In Equation (12): m —total number of specimens per group and i —experimental data arranged in order from small to large.

Through Equation (9) to Equation (12), with X as the abscissa and Y as the ordinate, the corresponding regression parameters a and b are obtained by linear fitting of the data, as shown in Table 5.

Table 5. Regression parameter values.

NO.	Regression Parameter		Regression Coefficient
SPRC-0-0	$a = -43.95136$	$b = 6.59925$	$R^2 = 0.91731$
SPRC-0.5-5	$a = -64.91919$	$b = 8.98057$	$R^2 = 0.89184$
SPRC-0.5-10	$a = -75.09988$	$b = 10.28831$	$R^2 = 0.95511$
SPRC-0.5-15	$a = -77.32255$	$b = 10.65826$	$R^2 = 0.9082$
SPRC-1-5	$a = -147.07487$	$b = 19.95748$	$R^2 = 0.95815$
SPRC-1-10	$a = -199.48323$	$b = 26.43486$	$R^2 = 0.95857$
SPRC-1-15	$a = -104.51039$	$b = 14.03187$	$R^2 = 0.82022$
SPRC-1.5-5	$a = -92.86202$	$b = 13.01777$	$R^2 = 0.97532$
SPRC-1.5-10	$a = -64.37724$	$b = 8.86828$	$R^2 = 0.91335$
SPRC-1.5-15	$a = -119.01573$	$b = 16.65037$	$R^2 = 0.951$

From Table 5, the maximum value of the regression coefficient R^2 for the concrete with compound silica fume and polyvinyl alcohol fiber is 0.97532. Most of the regression coefficients R^2 of the group are greater than 0.9, and a small number are less than 0.9, but greater than 0.82022. The linear regression fitting results are good, and the test results conform to the distribution law of the Weibull probability density function, which indicates that $Y = a + bX$ is valid.

Equation (13) can be obtained by deformation according to Equation (8) to Equation (12). The impact life of the SPRC under different failure probabilities P_1 is analyzed and estimated by Equation (13):

$$N = \exp \left\{ \frac{\ln[\ln(1/(1 - P_1))] - a}{b} \right\} \tag{13}$$

The parameters a and b in Equation (13) are obtained from Table 5, and the impact life at different failure probabilities P_1 can be found by Equation (13), and the estimated impact life of the SPRC at different failure probabilities P_1 is shown in Table 6.

Table 6. Impact life of each group of specimens under different failure probabilities (times).

NO.	$P_1 = 0.3$	$P_1 = 0.4$	$P_1 = 0.5$	$P_1 = 0.6$	$P_1 = 0.7$
SPRC-0-0	668	705	738	770	803
SPRC-0.5-5	1229	1279	1324	1365	1407
SPRC-0.5-10	1339	1386	1428	1467	1507
SPRC-0.5-15	1284	1328	1367	1403	1440
SPRC-1-5	1507	1534	1558	1580	1602
SPRC-1-10	1821	1846	1867	1887	1907
SPRC-1-15	1595	1636	1672	1706	1739
SPRC-1.5-5	1158	1190	1218	1245	1271
SPRC-1.5-10	1265	1318	1364	1407	1451
SPRC-1.5-15	1195	1221	1244	1265	1286

3.3.2. SPRC Impact-Damage Analysis

In the previous section, the impact life of SPRC with different failure probabilities was predicted using the Weibull probability density function, but the damage variation in the SPRC from the first impact load until impact damage occurred was not systematically studied. In this section, the macroscopic-damage evolution law of each group of specimens after repeated drop-hammer impacts was studied by establishing the SPRC impact-damage model using the Weibull distribution.

With the increase in drop-hammer-impact times, the function value of the Weibull distribution failure probability function also gradually increases, which is an increasing function. From the process of damage deterioration under impact loading, it is clear that the impact-damage degree of the concrete increases with the number of impacts, and with the superposition of impact damage to concrete from each impact load, the fatigue damage from impact loading is a growth process. It can be considered that the damage degree and failure probability accumulate simultaneously in the process of drop-hammer impact.

After n times hammer impacts, the failure probability of the concrete is $P_F(n)$, and the damage degree is $D(n)$. When the concrete fails by drop-hammer impact, the failure probability of concrete is $P_F(n) = 1$, and the damage degree is $D(n) = 1$. In summary, the impact-damage model of concrete based on the Weibull distribution can be expressed by Equation (14):

$$D(n) = 1 - \exp \left[- \left(\frac{n}{\eta} \right)^\beta \right] \tag{14}$$

where n is the number of impacts, β and η can be obtained by combining Equations (5)–(10) with Table 7 and substituting the calculation results into Equation (14), and the damage-evolution equation of each group of specimens under the action of impact loading can be derived, as shown in Table 7.

Table 7. SPRC impact-damage-evolution equation.

$SPFC - 0 - 0 : D(n) = 1 - \exp \left[- \left(\frac{n}{780.593} \right)^{6.599} \right]$	$SPFC - 0.5 - 5 : D(n) = 1 - \exp \left[- \left(\frac{n}{1378.636} \right)^{8.981} \right]$
$SPFC - 0.5 - 10 : D(n) = 1 - \exp \left[- \left(\frac{n}{1479.612} \right)^{10.288} \right]$	$SPFC - 0.5 - 15 : D(n) = 1 - \exp \left[- \left(\frac{n}{1414.748} \right)^{10.658} \right]$
$SPFC - 1 - 5 : D(n) = 1 - \exp \left[- \left(\frac{n}{1586.699} \right)^{19.957} \right]$	$SPFC - 1 - 10 : D(n) = 1 - \exp \left[- \left(\frac{n}{1893.569} \right)^{26.435} \right]$
$SPFC - 1 - 15 : D(n) = 1 - \exp \left[- \left(\frac{n}{1716.552} \right)^{14.032} \right]$	$SPFC - 1.5 - 5 : D(n) = 1 - \exp \left[- \left(\frac{n}{1253.232} \right)^{13.018} \right]$
$SPFC - 1.5 - 10 : D(n) = 1 - \exp \left[- \left(\frac{n}{1421.219} \right)^{8.87} \right]$	$SPFC - 1.5 - 15 : D(n) = 1 - \exp \left[- \left(\frac{n}{1271.475} \right)^{16.65} \right]$

According to the impact-damage-evolution equation in Table 7, the damage evolution of each group of specimens versus impact damage is plotted in Figure 6. The trend of the SPRC impact-damage evolution under repeated impact loadings can be seen. In the early stage of impact damage, the expansion of pores and the extension of microcracks in concrete are small, and the damage deterioration is low. With the increasing number of impacts, the expansion of small pores in concrete and the extension of microcracks increase. The damage and deterioration of the concrete become increasingly severe, and the increase in the loss degree gradually increases. When the loss degree $D(N) = 1$, the concrete is completely destroyed. Figure 6 shows that, in the data results derived from the impact-damage-evolution equation, the impact-damage-life law of concrete is highly consistent with the test results, indicating that the impact-damage-evolution equation established based on the Weibull distribution model can well reflect the impact-damage-evolution trend of SPRC under repeated impact loading.

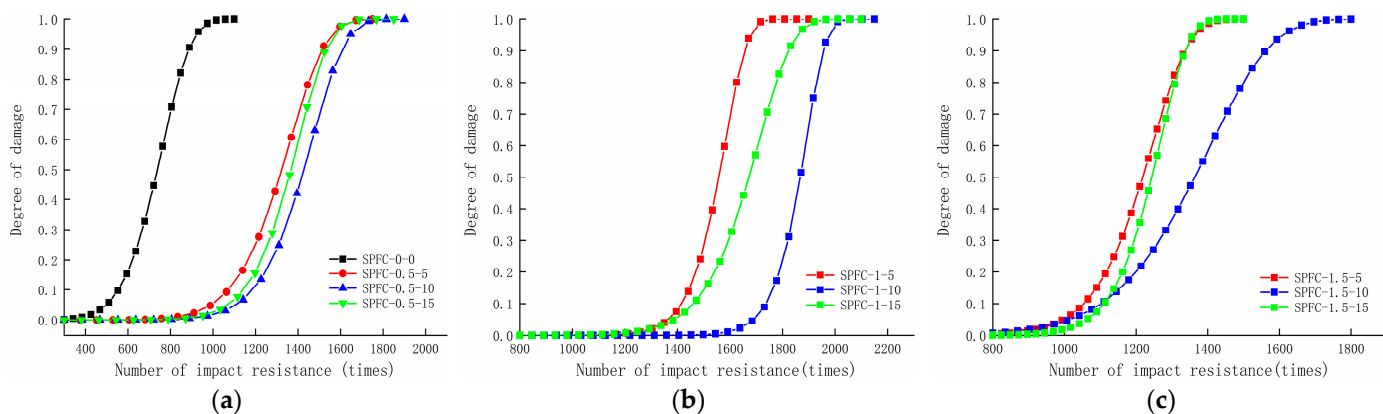


Figure 6. SPRC specimen impact-damage-evolution diagram (a) Impact-damage-evolution diagram of specimens with 0 and 0.5% polyvinyl alcohol fiber content; (b) Impact-damage-evolution diagram of specimens with 1% polyvinyl alcohol fiber content; (c) Impact-damage-evolution diagram of specimens with 1.5% polyvinyl alcohol fiber content.

3.4. Analysis of the Impact Life of the SFPC Based on the RSM under Different Failure Probabilities

3.4.1. Factor Level and Response

Response surface method (RSM) is an optimization method that responds to core elements by multiple factors [52]. The functional relationships are displayed graphically for direct observation to select the optimal conditions in an experimental design. The RSM can analyze the obviousness of the test results, obtain the optimal test scheme, and effectively predict the test results. To further explore the effects of silica-fume content, polyvinyl-alcohol-fiber content and failure probability on the impact resistance of SPRC, RSM was used to analyze the impact resistance of SPRC under the interaction of different factors and contents. Considering the single-factor effect and the two-factor interaction effect, the quadratic response surface equation can be established, as shown in Equation (15). The impact life of SPRC was analyzed by RSM with Factor A (silica-fume content), Factor B (polyvinyl-alcohol-fiber content) and Factor C (failure probability). The factors and level variations are shown in Table 8.

$$R = \alpha_0 + \sum_{i=1}^n \alpha_i X_i + \sum_{i=1}^n \alpha_{ii} X_i^2 + \sum_{i<j}^n a_{ij} X_i X_j + \varepsilon \quad (X_i, X_i, \dots, X_i) \quad (15)$$

Table 8. Factor and factor level.

Factor	Factor Level		
	−1	0	1
Silica fume content (%)	5	10	15
Polyvinyl alcohol fiber content (%)	0.5	1	1.5
Probability of failure	0	0.5	1

In Equation (15), *R* is the response function (also called the objective function) for independent variable factor *X_i*; α_i , α_{ii} , α_{ij} are the regression coefficients of the primary term coefficient, the secondary term coefficient and the interaction term, respectively; *n* is the number of influencing factors; and ε is the error (experimental error and fitting error).

3.4.2. Establishment of the RSM Model

RSM analysis design and results are shown in Table 9. The quadratic surface regression model was obtained by fitting multiple regression analysis to the experimental data using Design-Expert software, as shown in Equation (16). Variance analysis was carried out on Equation (16) of the model. The *F* value and *P* value of the model are used to test the

significance and effectiveness of the model. The F value and P value of the lack of fit are used to test another basis for whether the model is effectiveness. The regression coefficient R^2 value is used to test the reliability of the model. When the P value of the model is less than 0.05 and the P value of the lack of fit is greater than 0.05, the model has high significance. When the value of the regression coefficient R^2 is closer to 1 and the C.V. is less than 10%, the model has a high reliability.

$$R = 1870.2 + 24.25A - 40.38B + 647.88C - 4.25AB + 98.75AC + 24BC - 186.6A^2 - 395.35B^2 - 301.85C^2 \quad (16)$$

Table 9. RSM analysis design and results.

NO.	Experimental Design			Results/Times
	A/%	B/%	C	
1	5.00	1.00	0.00	891
2	10.00	1.00	0.50	1867
3	5.00	0.50	0.50	1324
4	10.00	1.00	0.50	1928
5	5.00	1.00	1.00	1810
6	5.00	1.50	0.50	1218
7	15.00	1.00	0.00	756
8	15.00	1.00	1.00	2070
9	10.00	1.00	0.50	1887
10	10.00	1.00	0.50	1762
11	15.00	1.50	0.50	1244
12	10.00	0.50	1.00	1910
13	10.00	1.50	1.00	1911
14	10.00	1.00	0.50	1907
15	15.00	0.50	0.50	1367
16	10.00	1.50	0.00	388
17	10.00	0.50	0.00	483

The variance analysis of the impact life response model of the SPRC is shown in Table 10. As seen in Table 10, the P value of the model is much less than 0.05 and the P value of the lack of fit is 0.0696, which is greater than 0.05. This indicates that the model has high significance and effectiveness, reflecting the high correlation between the model and the experimental data. In addition the regression coefficient R^2 value of the model is 0.9826 and the C.V. value is 7.52%, which indicates that the model has good reliability. Based on the above significance and reliability tests, this model can reasonably describe and predict the impact life of SPRC under the interaction of silica-fume content, polyvinyl-alcohol-fiber content and different failure probabilities.

Table 10. Variance analysis of the SPRC impact-life response model.

Source	Sun of Squares	Mean of Squares	F Value	p Value
Model	4.73×10^6	5.225×10^5	43.99	<0.0001
A	4704.5	4704.5	0.39	0.5502
B	13,041.13	13,041.13	1.09	0.3308
C	3.358×10^6	3.358×10^6	281.08	<0.0001
AB	72.25	72.25	6.048×10^{-3}	0.9402
AC	39,006.25	39,006.25	3.27	0.1137
BC	2304	2304	0.19	0.6738
A2	1.466×10^5	1.466×10^5	12.27	0.0100
B2	6.581×10^5	6.581×10^5	55.09	0.0001
C2	3.836×10^5	3.836×10^5	32.11	0.0008
Lack of Fit	66,931.25	22,310.42	5.35	0.0696

3.4.3. RSM Model Results Analysis

The RSM scheme was imported into Design-Expert to analyze the effect of the variation in Factor A (silica-fume dosing), Factor B (polyvinyl-alcohol-fiber dosing) and Factor C (failure probability) on the significance of the impact life of SPFC. The contour map and 3D response surface map derived from the model are shown in Figure 7.

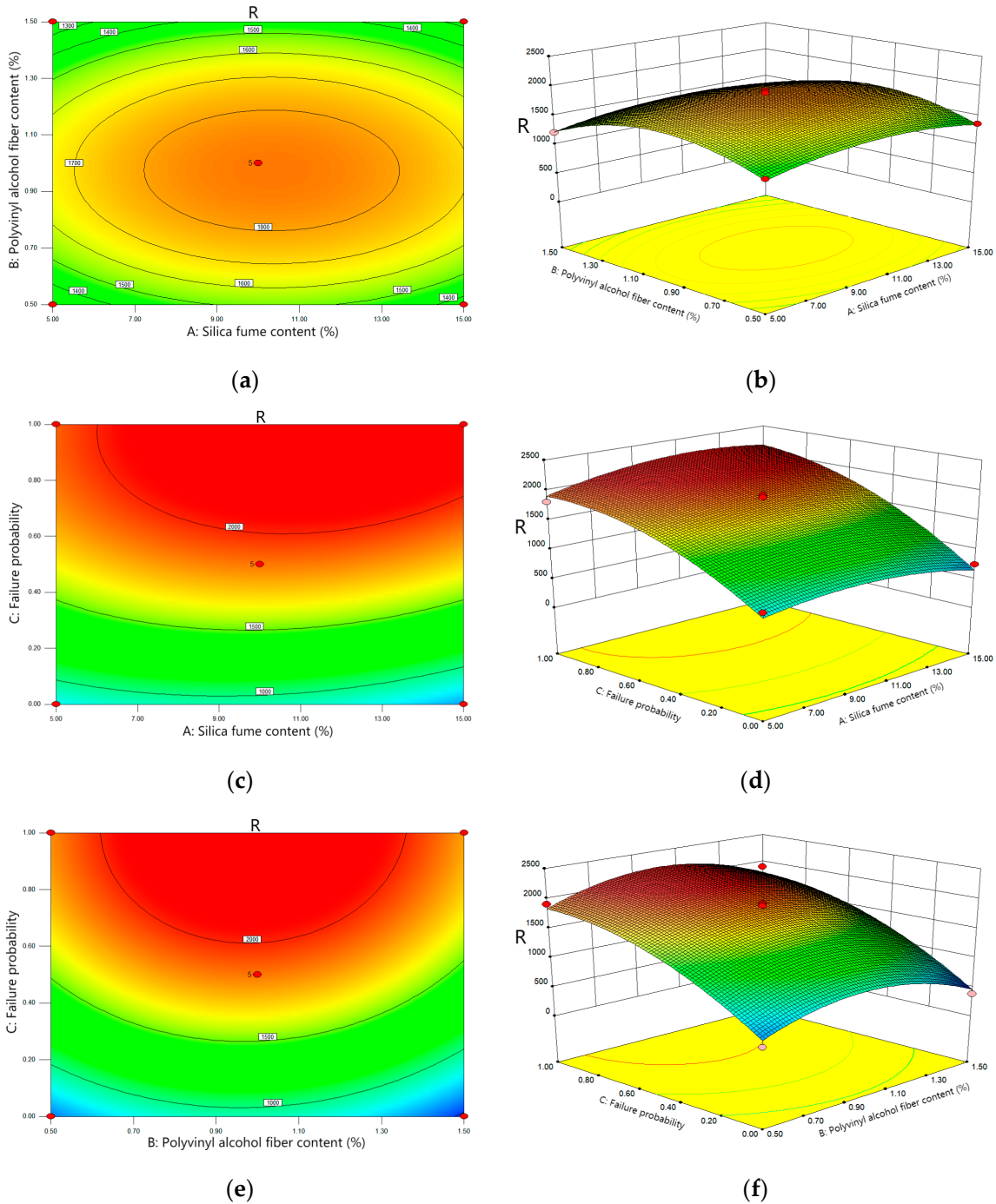


Figure 7. Effects of Factor A, B, C and their interactions on R. (a,b): Effects of Factor A and B and their interactions on R; (c,d): Effects of Factor A and C and their interactions on R; (e,f): Effects of Factor B and C and their interactions on R.

Through the analysis of Figure 7a,b, the contour map shows that the surrounding green gradually transforms into orange at the center, and the center is the region with

the highest response degree, which indicates that the corresponding material content in this region is the optimal doping value. In the 3D response surface diagram, the trend of the R value along Factor B is greater than that of Factor A, which indicates that Factor B (polyvinyl-alcohol-fiber content) has a higher effect on R values than factor A (silica-fume content).

As seen from Figure 7c,d, in the contour map, it can be seen that the green below gradually changes to the red above. The top right area is the highest response area, and the corresponding failure probability and silica-fume content are the best values. Compared with Factor A, the trend of R value along Factor C is more obvious in the 3D response surface diagram, which indicates that Factor C (failure probability) has greater influence on R values than Factor A (silica-fume content).

As seen from Figure 7e,f, the contour map shows that the green below gradually changes to the red above. The central area above is the area with the highest response, and the corresponding failure probability and polyvinyl-alcohol-fiber content are the best values. Compared with Factor B, the trend of the R value along Factor C is more obvious in the three-dimensional response surface diagram, which indicates that the influence of Factor C (the failure probability) has a greater effect on the R value than that of Factor B (polyvinyl-alcohol-fiber content).

4. Conclusions

SPRC was prepared and tested for compressive strength and impact resistance, and the results were analyzed in depth using the Weibull distribution model and RSM. The following conclusions can be drawn from the results obtained:

1. With the increase in silica-fume and polyvinyl-alcohol-fiber content, the compressive strength and impact energy dissipation of SPRC first increase and then decrease. When the silica-fume content is 10% and the polyvinyl-alcohol-fiber content is 1%, the compressive strength and impact resistance of SPRC are the best, and these values are 26.6% and 154.23% higher than those of the benchmark concrete, respectively.
2. The SPRC impact life test results obey the Weibull distribution probability density function well; thus, the Weibull distribution model can be used to effectively predict the impact life of SPRC under different failure probabilities.
3. The equation of the SPRC impact damage evolution is established based on the Weibull distribution model. The predicted values of the model are in high consistency with the experimental results. This indicates that the model has high reliability and can accurately describe the damage degradation process of the SPFC under repeated impact loading.
4. The RSM model was established by combining the level changes of the three factors. The results show that the model has high significance, validity and reliability. Therefore, the impact life of SPRC under the action of these three factors can be effectively predicted.

Author Contributions: Conceptualization, S.C., Z.X., Z.L., C.W. and J.J.; methodology and data curation, S.C. and Z.X.; validation and investigation, S.C., Z.L. and C.W.; formal analysis, S.C., Z.X.; resources, J.J.; writing—original draft preparation, S.C.; writing—review and editing, Z.X. and J.J.; supervision, J.J.; and funding acquisition, J.J. All authors have read and agreed to the published version of the manuscript.

Funding: This research received no external funding.

Institutional Review Board Statement: Not applicable.

Informed Consent Statement: Not applicable.

Data Availability Statement: The data used to support the findings of this study are available from the corresponding author upon request.

Acknowledgments: The authors acknowledge the Hubei University of Technology for funding this research.

Conflicts of Interest: The authors declare no conflict of interest.

References

1. Wang, L.; Li, G.; Li, X.; Guo, F.; Tang, S.; Lu, X.; Hanif, A. Influence of reactivity and dosage of MgO expansive agent on shrinkage and crack resistance of face slab concrete. *Cem. Concr. Compos.* **2021**, *126*, 104333. [[CrossRef](#)]
2. Wang, L.; Zeng, X.; Yang, H.; Lv, X.; Guo, F.; Shi, Y.; Hanif, A. Investigation and Application of Fractal Theory in Cement-Based Materials: A Review. *Fractal Fract.* **2021**, *5*, 247. [[CrossRef](#)]
3. Law, S.; Zhu, X. Dynamic behavior of damaged concrete bridge structures under moving vehicular loads. *Eng. Struct.* **2004**, *26*, 1279–1293. [[CrossRef](#)]
4. Madrazo-Aguirre, F.; Ruiz-Teran, A.M.; Wadee, M.A. Dynamic behaviour of steel–concrete composite under-deck cable-stayed bridges under the action of moving loads. *Eng. Struct.* **2015**, *103*, 260–274. [[CrossRef](#)]
5. Jiang, C.; Wu, C.; Cai, C.; Xiong, W. Fatigue analysis of stay cables on the long-span bridges under combined action of traffic and wind. *Eng. Struct.* **2020**, *207*, 110212. [[CrossRef](#)]
6. Zhang, D.; Cai, L.; Zhou, S. An Airfield Soil Pavement Design Method Based on Rut Depth and Cumulative Fatigue. *J. Adv. Transp.* **2019**, *2019*, 1–11. [[CrossRef](#)]
7. Wang, S.; Garbatov, Y.; Chen, B.; Soares, C.G. Dynamic structural response of perforated plates subjected to water impact load. *Eng. Struct.* **2016**, *125*, 179–190. [[CrossRef](#)]
8. Kwag, S.; Gupta, A.; Baugh, J.; Kim, H.-S. Significance of multi-hazard risk in design of buildings under earthquake and wind loads. *Eng. Struct.* **2021**, *243*, 112623. [[CrossRef](#)]
9. Tian, Z.-L.; Liu, Y.-L.; Zhang, A.-M.; Tao, L.; Chen, L. Jet development and impact load of underwater explosion bubble on solid wall. *Appl. Ocean Res.* **2019**, *95*, 102013. [[CrossRef](#)]
10. Wang, J.-P.; Su, J.-B.; Wu, F.; Zhang, Z.; Lv, Y. Lateral dynamic load tests of offshore piles based using the m-method. *Ocean Eng.* **2020**, *220*, 108413. [[CrossRef](#)]
11. Li, Z.; Escoffier, S.; Kotronis, P. Study on the stiffness degradation and damping of pile foundations under dynamic loadings. *Eng. Struct.* **2019**, *203*, 109850. [[CrossRef](#)]
12. Bayraktar, A.; Hançer, E.; Akköse, M. Influence of base-rock characteristics on the stochastic dynamic response of dam–reservoir–foundation systems. *Eng. Struct.* **2005**, *27*, 1498–1508. [[CrossRef](#)]
13. Zhang, M.H.; Sharif, M.S.H.; Lu, G. Impact resistance of high-strength fibre-reinforced concrete. *Mag. Concr. Res.* **2007**, *59*, 199–210. [[CrossRef](#)]
14. Yoo, D.-Y.; Yoon, Y.-S. Influence of steel fibers and fiber-reinforced polymers on the impact resistance of one-way concrete slabs. *J. Compos. Mater.* **2014**, *48*, 695–706. [[CrossRef](#)]
15. Zhang, M.; Shim, V.; Lu, G.; Chew, C. Resistance of high-strength concrete to projectile impact. *Int. J. Impact Eng.* **2004**, *31*, 825–841. [[CrossRef](#)]
16. Wu, H.; Fang, Q.; Gong, J.; Liu, J.; Zhang, J.; Gong, Z. Projectile impact resistance of corundum aggregated UHP-SFRC. *Int. J. Impact Eng.* **2015**, *84*, 38–53. [[CrossRef](#)]
17. Mastali, M.; Dalvand, A.; Sattarifard, A. The impact resistance and mechanical properties of reinforced self-compacting concrete with recycled glass fibre reinforced polymers. *J. Clean. Prod.* **2016**, *124*, 312–324. [[CrossRef](#)]
18. Karimipour, A.; Ghalehnovi, M.; de Brito, J.; Attari, M. The effect of polypropylene fibres on the compressive strength, impact and heat resistance of self-compacting concrete. In *Structures*; Elsevier: Amsterdam, The Netherlands, 2020; Volume 25, pp. 72–87. [[CrossRef](#)]
19. Ahmed, S.; Ali, M. Use of agriculture waste as short discrete fibers and glass-fiber-reinforced-polymer rebars in concrete walls for enhancing impact resistance. *J. Clean. Prod.* **2020**, *268*, 122211. [[CrossRef](#)]
20. Zhang, F.; Poh, L.H.; Zhang, M.-H. Effect of bauxite aggregate in cement composites on mechanical properties and resistance against high-velocity projectile impact. *Cem. Concr. Compos.* **2021**, *118*, 103915. [[CrossRef](#)]
21. Mustafa, M.A.-T.; Hanafi, I.; Mahmoud, R.; Tayeh, B. Effect of partial replacement of sand by plastic waste on impact resistance of concrete: Experiment and simulation. *Structures* **2019**, *20*, 519–526. [[CrossRef](#)]
22. Vatin, N.I.; Murali, G.; Abid, S.R.; de Azevedo, A.R.G.; Tayeh, B.A.; Dixit, S. Enhancing the Impact Strength of Prepacked Aggregate Fibrous Concrete Using Asphalt-Coated Aggregates. *Materials* **2022**, *15*, 2598. [[CrossRef](#)]
23. Kalkan, E.; Akbulut, S. The positive effects of silica fume on the permeability, swelling pressure and compressive strength of natural clay liners. *Eng. Geol.* **2004**, *73*, 145–156. [[CrossRef](#)]
24. Xi, J.; Liu, J.; Yang, K.; Zhang, S.; Han, F.; Sha, J.; Zheng, X. Role of silica fume on hydration and strength development of ultra-high performance concrete. *Constr. Build. Mater.* **2022**, *338*, 127600. [[CrossRef](#)]
25. Luan, C.; Wang, J.; Gao, J.; Wang, J.; Du, P.; Zhou, Z.; Huang, Y.; Du, S. Changes in fractal dimension and durability of ultra-high performance concrete (UHPC) with silica fume content. *Arch. Civ. Mech. Eng.* **2022**, *22*, 1–17. [[CrossRef](#)]
26. Poon, C.; Kou, S.; Lam, L. Compressive strength, chloride diffusivity and pore structure of high performance metakaolin and silica fume concrete. *Constr. Build. Mater.* **2006**, *20*, 858–865. [[CrossRef](#)]

27. Hassani, A.; Arjmandi, M. Enhancement of concrete properties for pavement slabs using waste metal drillings and silica fume. *Waste Manag. Res. J. Sustain. Circ. Econ.* **2010**, *28*, 56–63. [[CrossRef](#)]
28. Alaloul, W.; Musarat, M.; Haruna, S.; Law, K.; Tayeh, B.; Rafiq, W.; Ayub, S. Mechanical Properties of Silica Fume Modified High-Volume Fly Ash Rubberized Self-Compacting Concrete. *Sustainability* **2021**, *13*, 5571. [[CrossRef](#)]
29. Liu, H.; Luo, G.; Zhou, P.; Wei, H.; Li, W.; Yu, D. Flexural-Fatigue Properties of Sustainable Pervious Concrete Pavement Material Containing Ground Tire Rubber and Silica Fume. *Sustainability* **2019**, *11*, 4467. [[CrossRef](#)]
30. Zhao, S.; Zhang, Q. Effect of Silica Fume in Concrete on Mechanical Properties and Dynamic Behaviors under Impact Loading. *Materials* **2019**, *12*, 3263. [[CrossRef](#)]
31. Shafaghat, J.; Allahverdi, A. Enhancing Concrete Properties by Using Silica Fume as Reactive Powder and Portland Cement-Clinker as Reactive Aggregate. *J. Mater. Civ. Eng.* **2019**, *31*, 04019278. [[CrossRef](#)]
32. Feng, J.; Sun, W.; Zhai, H.; Wang, L.; Dong, H.; Wu, Q. Experimental Study on Hybrid Effect Evaluation of Fiber Reinforced Concrete Subjected to Drop Weight Impacts. *Materials* **2018**, *11*, 2563. [[CrossRef](#)] [[PubMed](#)]
33. Shao, Y.; Okubo, K.; Fujii, T.; Shibata, O.; Fujita, Y. Effect of physical modification of matrix by nano(polyvinyl alcohol) fibers on fatigue performance of carbon fiber fabric-reinforced vinylester composites. *J. Compos. Mater.* **2016**, *50*, 4065–4075. [[CrossRef](#)]
34. Sun, M.; Chen, Y.; Zhu, J.; Sun, T.; Shui, Z.; Ling, G.; Zhong, H. Effect of Modified Polyvinyl Alcohol Fibers on the Mechanical Behavior of Engineered Cementitious Composites. *Materials* **2018**, *12*, 37. [[CrossRef](#)] [[PubMed](#)]
35. Li, D.; Hai, C.; Jinping, O. Fracture behavior and damage evaluation of polyvinyl alcohol fiber concrete using acoustic emission technique. *Mater. Des.* **2012**, *40*, 205–211. [[CrossRef](#)]
36. Zhang, R.; Jin, L.; Tian, Y.; Dou, G.; Du, X. Static and dynamic mechanical properties of eco-friendly polyvinyl alcohol fiber-reinforced ultra-high-strength concrete. *Struct. Concr.* **2019**, *20*, 1051–1063. [[CrossRef](#)]
37. Qiu, J.; Ni Lim, X.; Yang, E.-H. Fatigue-induced in-situ strength deterioration of micro-polyvinyl alcohol (PVA) fiber in cement matrix. *Cem. Concr. Compos.* **2017**, *82*, 128–136. [[CrossRef](#)]
38. Kim, B.; Boyd, A.; Lee, J.Y. Durability performance of fiber-reinforced concrete in severe environments. *J. Compos. Mater.* **2011**, *45*, 2379–2389. [[CrossRef](#)]
39. Afroughsabet, V.; Teng, S. Experiments on drying shrinkage and creep of high performance hybrid-fiber-reinforced concrete. *Cem. Concr. Compos.* **2020**, *106*, 103481. [[CrossRef](#)]
40. Chen, L.; Sun, W.; Chen, B.; Xu, S.; Liang, J.; Ding, C.; Feng, J. A Comparative Study on Blast-Resistant Performance of Steel and PVA Fiber-Reinforced Concrete: Experimental and Numerical Analyses. *Crystals* **2020**, *10*, 707. [[CrossRef](#)]
41. Zhao, N.; Wang, S.; Quan, X.; Xu, F.; Liu, K.; Liu, Y. Behavior of polyvinyl alcohol fiber reinforced geopolymer composites under the coupled attack of sulfate and freeze-thaw in a marine environment. *Ocean Eng.* **2021**, *238*, 109734. [[CrossRef](#)]
42. Mosavinejad, S.G.; Langaroudi, M.A.M.; Barandoust, J.; Ghanizadeh, A. Electrical and microstructural analysis of UHPC containing short PVA fibers. *Constr. Build. Mater.* **2020**, *235*, 117448. [[CrossRef](#)]
43. Prakash, S.; Kumar, S.; Biswas, R.; Rai, B. Influence of silica fume and ground granulated blast furnace slag on the engineering properties of ultra-high-performance concrete. *Innov. Infrastruct. Solut.* **2021**, *7*, 1–18. [[CrossRef](#)]
44. Singh, S.; Kaur, G. Impact resistance of waste tyre rubber and silica fume-based concrete mixes. *Int. J. Struct. Eng.* **2021**, *12*, 1–13. [[CrossRef](#)]
45. Suruchi, M.; Sharma, H.K. Impact resistance and mechanical properties of UHPFRC. *Iran. J. Sci. Technol. Trans. Civ. Eng.* **2019**, *43*, 371–380. [[CrossRef](#)]
46. *GB/T 50081-2019*; Standard for Test Methods of Concrete Physical and Mechanical Properties. Ministry of Housing and Urban-Rural Development of the People's Republic of China; China Architecture & Building Press: Beijing, China, 2019.
47. *CECS 13:2009*; Standard Test Methods for Fiber Reinforced Concrete. China Planning Press: Beijing, China, 2009.
48. ACI Committee 544. Measurement of Properties of Fiber Reinforced Concrete. *ACI Mater. J.* **1998**, *85*, 83–93.
49. Ai, Y.; Zhu, S.P.; Liao, D.; Correia, J.A.F.O.; Souto, C.; De Jesus, A.M.P.; Keshtegar, B. Probabilistic modeling of fatigue life distribution and size effect of components with random defects. *Int. J. Fatigue* **2019**, *126*, 165–173. [[CrossRef](#)]
50. Zhu, Z.; Zhang, C.; Meng, S.; Shi, Z.; Tao, S.; Zhu, D. A Statistical Damage Constitutive Model Based on the Weibull Distribution for Alkali-Resistant Glass Fiber Reinforced Concrete. *Materials* **2019**, *12*, 1908. [[CrossRef](#)]
51. Strzelecki, P. Determination of fatigue life for low probability of failure for different stress levels using 3-parameter Weibull distribution. *Int. J. Fatigue* **2021**, *145*, 106080. [[CrossRef](#)]
52. Siamardi, K.; Shabani, S. Evaluation the effect of micro-synthetic fiber on mechanical and freeze-thaw behavior of non-air-entrained roller compacted concrete pavement using response surface methodology. *Constr. Build. Mater.* **2021**, *295*, 123628. [[CrossRef](#)]